論文 / 著書情報
Article / Book Information

Title	Mask 3D Parameter Prediction in EUV Lithography by Convolutional Neural Network
Authors	Atsushi Takahashi, Moe Sugiyama, Masayuki Shimoda, Hiroyoshi Tanabe
Citation	IEEE Asia Pacific Conference on Circuits and Systems (APCCAS)
Pub. date	2025, 10
Copyright	(c) 2025 IEEE. Personal use of this material is permitted. Permission from IEEE must be obtained for all other uses, in any current or future media, including reprinting/republishing this material for advertising or promotional purposes, creating new collective works, for resale or redistribution to servers or lists, or reuse of any copyrighted component of this work in other works.
DOI	http://dx.doi.org/10.1109/APCCAS67402.2025.11378293
Note	This file is author (final) version.

Mask 3D Parameter Prediction in EUV Lithography by Convolutional Neural Network

Atsushi Takahashi
Institute of Science Tokyo
Tokyo, Japan
atsushi@ict.eng.isct.ac.jp

Moe Sugiyama
Institute of Science Tokyo
Tokyo, Japan
sugiyama@eda.ict.eng.isct.ac.jp

Masayuki Shimoda
Institute of Science Tokyo
Tokyo, Japan
shimoda@ict.eng.isct.ac.jp

Hiroyoshi Tanabe
Institute of Science Tokyo
Tokyo, Japan
tanabe@eda.ict.eng.isct.ac.jp

***Abstract*—In extreme ultraviolet (EUV) lithography, a rigorous but time-consuming electromagnetic simulation is conventionally used to obtain the diffraction amplitude from an EUV mask. This is because the absorber thickness of the mask is comparable to the pattern size and the mask 3D effect is non-negligible. In our research, the diffraction amplitude is divided into the thin mask amplitudes and the residual mask 3D amplitude. The mask 3D amplitude is a function of the incident angle and the diffraction order, and the incident angle dependence of the mask 3D amplitude is approximated by a linear function using mask 3D parameters. Mask 3D parameters represent the on-axis and the off-axis mask 3D effects. The number of parameters that need to be predicted is more than ten thousand, and these parameters are predicted by convolutional neural networks from an input mask pattern. The image intensity on the wafer estimated using the mask 3D parameters predicted by the convolutional neural network is obtained 3,000 times faster than the electromagnetic simulation.**

***Index Terms*—lithography simulation, neural network, extreme ultraviolet mask**

I. Introduction

With the advancement of semiconductor integrated circuits, research and development of various manufacturing and design technologies is progressing. Among them, lithography is a key technology that drives miniaturization. To achieve miniaturization, the light source of the exposure tool has been shortened from the g-line and i-line of a mercury lamp to KrF and ArF excimer lasers. In the most advanced exposure tool, extreme ultraviolet (EUV) light with a wavelength of 13.5 nm is used.

The optical system of the conventional exposure tool was a transmission type using a lens, but since there is no optical material that transmits EUV light, the optical system of the EUV exposure tool is a reflection type using a mirror. As with the optical system, a reflection type is also used for the EUV mask. The incident light on the transmission type mask is vertical, but the incident light on the EUV mask is tilted because it is a reflection type. When light is incident from an oblique direction, the mask 3D (M3D) effect occurs due to the three-dimensional structure of the mask pattern.

Even with conventional optical exposure, there was a mismatch between the mask pattern and the printed pattern on the wafer. This is because when printing a pattern that is finer than the wavelength of the light source, the optical image becomes blurred. Since the late 1990s, technology has been developed to correct the mask pattern to bring the printed pattern closer to the design pattern. This is called optical proximity correction (OPC) [1].

Early OPC relied on rule-based methods for mask pattern correction. To improve accuracy, model-based OPC using lithography simulation was developed and is now standard [2]–[5]. This required faster lithography simulation, achieved through both faster computers and improved algorithms. In [6]–[8], fast compensation techniques for optical lithography simulation were introduced to improve the accuracy of the estimation obtained by rough simulation.

Optical lithography simulation uses Fourier transformation (FT) to obtain the diffraction amplitude from the mask. On the other hand, due to the mask 3D effect, EUV lithography simulation requires computationally expensive electromagnetic (EM) simulations. This limits full-mask OPC in EUV, making it practical only for local corrections. To make full-mask OPC in EUV possible, fast compensation techniques to avoid time-consuming EM simulations are needed.

In this paper, efforts to accurately obtain the diffraction amplitude from an EUV mask by convolutional neural networks (CNNs) so far [9]–[21] are summarized. Our research uses deep learning to accelerate EUV lithography simulation, including the M3D effect.

In order to accurately estimate the diffraction amplitude in a short time, the diffraction amplitude is divided into the thin mask amplitudes (Fourier transformation of the mask pattern) and the residual mask 3D amplitude [9]–[11], [21]. The mask 3D amplitude is a function of the incident angle and the diffraction order. The incident angle dependence of the mask 3D amplitude is approximated by a linear function using mask 3D parameters which represent the on-axis and the off-axis mask 3D effects [21]. A data augmentation technique to train CNNs effectively was introduced in [12], [13]. The potentials and the limitations of CNN for EUV simulation were discussed using imec 3 nm node (iN3) mask patterns in [14], [15]. Techniques to shorten the preparation time of training data for CNNs by weakly guiding approximation in EM simulation were introduced in [16], [17], [19]. Also, techniques to shorten the training time of CNNs were introduced [18]. The dependence of the mask 3D effects on the numerical aperture (NA) and the mask absorber is discussed in [20].

In the following, mask 3D parameters and CNNs for mask 3D parameter prediction in EUV lithography are introduced.

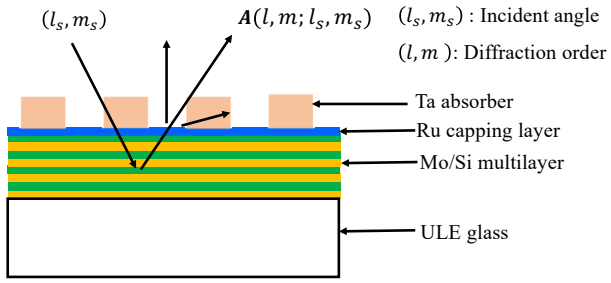

Fig. 1: Cross sectional view of an EUV mask.

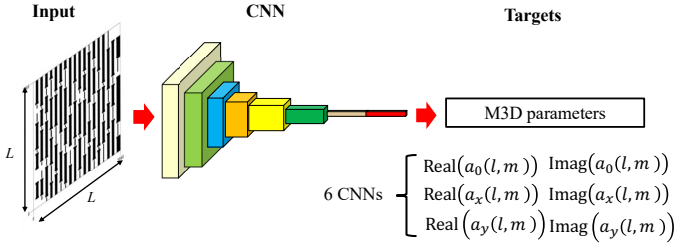

Fig. 2: CNN architecture.

II. Mask 3D Parameters

A. EUV mask structure

Figure 1 shows a cross-sectional view of an EUV mask. Ultra-low expansion (ULE) glass is used as a substrate. Mo/Si multilayer, which reflects EUV light, is formed on the ULE glass. The top of the Mo/Si multilayer is protected from oxidization by a thin Ru capping layer. Ta absorber, which absorbs EUV light, is formed on the Ru capping layer. The absorber is patterned by direct electron beam writing and etching in the mask manufacturing process. Typical height of Ta absorber is 60 nm. The resolution of the current EUV scanners is ∼15 nm. The magnification of the mask is four and the mask pattern size is ∼60 nm. Therefore, the aspect ratio of the absorber is ∼1, which causes a large M3D effect.

B. Linear approximation of the diffraction amplitude

Inside an EUV exposure tool the mask is illuminated from various incident angles (l_s, m_s) and the light is diffracted by the mask. The diffraction amplitude $\boldsymbol{A}$ depends on both the incident angle (l_s, m_s) and the diffraction order (l, m). EM simulation is required to obtain the diffraction amplitude $\boldsymbol{A}$ including the M3D effect. EM simulation is very slow. It takes about five minutes for a 512 nm × 512 nm area with Intel Core i9-10920X CPU and Nvidia RTX3090 GPU [21].

In our researches [9]–[11], [21], the diffraction amplitude is divided into thin mask amplitude (Fourier transformation of the mask pattern) $\boldsymbol{A}^{\mathrm{FT}}$ and residual M3D amplitude $\boldsymbol{A}^{\mathrm{3D}}$, and represented as follows:

$$\boldsymbol{A}(l, m; l_s, m_s) = \boldsymbol{A}^{\mathrm{FT}}(l, m) + \boldsymbol{A}^{\mathrm{3D}}(l, m; l_s, m_s).$$

Thin mask amplitude $\boldsymbol{A}^{\mathrm{FT}}$ can be obtained very fast by FT. It is the dominant part of the diffraction amplitude $\boldsymbol{A}$. The contribution of the M3D amplitude $\boldsymbol{A}^{\mathrm{3D}}$ is small but not negligible. It smoothly depends on the incident angle (l_s, m_s). This dependence is approximated by a linear function of l_s and m_s as follows [21]:

$$A^{\mathrm{3D}}(l, m; l_s, m_s) \simeq a_0(l, m) + a_x(l, m)\left(l_s + \frac{l}{2}\right) + a_y(l, m)\left(m_s + \frac{m}{2}\right).$$

Constant $a_0(l, m)$ and coefficients $a_x(l, m)$ and $a_y(l, m)$ are called M3D parameters. These parameters are the key metrics of the M3D effect.

III. Convolutional Neural Network for Mask 3D Parameters

In this section, convolutional neural networks (CNNs) that predict M3D parameters from an input mask pattern we developed in [21] are introduced. It enables us to replace the EM simulation with the CNN prediction, which significantly accelerates the EUV lithography simulation.

A. CNN architecture

The input of the CNN is a mask pattern, and the outputs are M3D parameters (Fig. 2).

The total number of M3D parameters is 5,399 where the number of a_0's is 1,901 and the numbers of a_x's and a_y's are both 1,749. The larger the number of targets, the harder it is to build a CNN with high accuracy. In our implementation, six CNNs for $\mathrm{Re}(a_0(l, m))$, $\mathrm{Im}(a_0(l, m))$, $\mathrm{Re}(a_x(l, m))$, $\mathrm{Im}(a_x(l, m))$, $\mathrm{Re}(a_y(l, m))$, and $\mathrm{Im}(a_y(l, m))$ are constructed. The total number of outputs by six CNNs is 10,798.

The input mask pattern is 2,048 × 2,048 binary data. It is first converted to 512 × 512 grayscale values by averaging the data. This is the input to CNN. Inside CNN, convolution, max pooling, and batch normalization are repeated five times. After flattening, two dense layers are added before the output.

B. CNN training

Figure 3 shows Manhattan mask patterns used for the training of CNNs. Type A, B, C, D, and E include random L/S patterns, 14 nm V lines, 14 nm H lines, 14 nm V lines with OPC, and 14 nm H lines with OPC, respectively. Both the bright field (BF) patterns and the dark field (DF) patterns are included. The size of the mask pattern is 512 nm × 512 nm on the wafer. 2,000 original mask patterns are generated for each mask type. Then, a data augmentation technique [12], [13] is used to increase the amount of data by a factor of 50. In the dataset, there are 100 thousand data for each mask type and one million data in total.

Figure 4 shows the training and validation losses of six CNNs during the training. For the validation, 500 mask patterns are generated for each mask type. The total number of the validation data is 5,000. Both the training and validation losses become small after the training. It is confirmed that CNNs successfully recognize the characteristics of Manhattan mask patterns. The training time takes about 40 hours for each CNN [21].

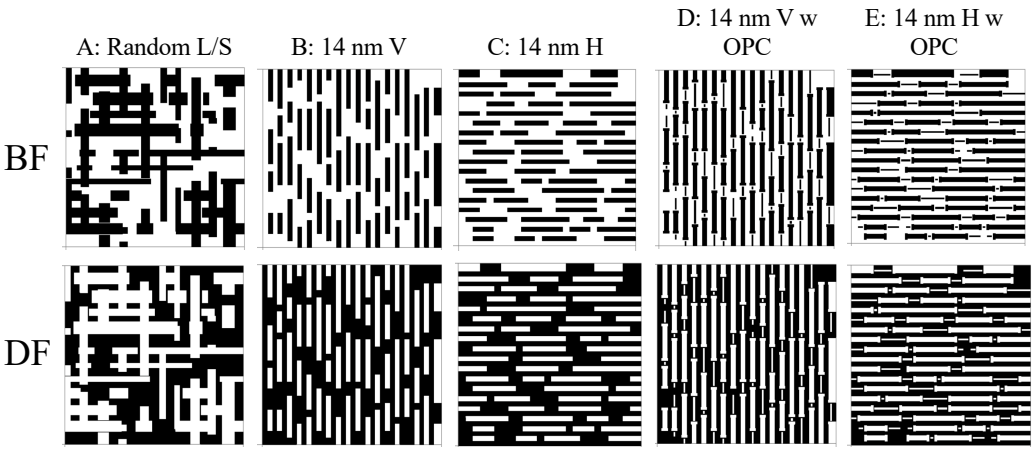

Fig. 3: Mask patterns used for the training of CNNs.

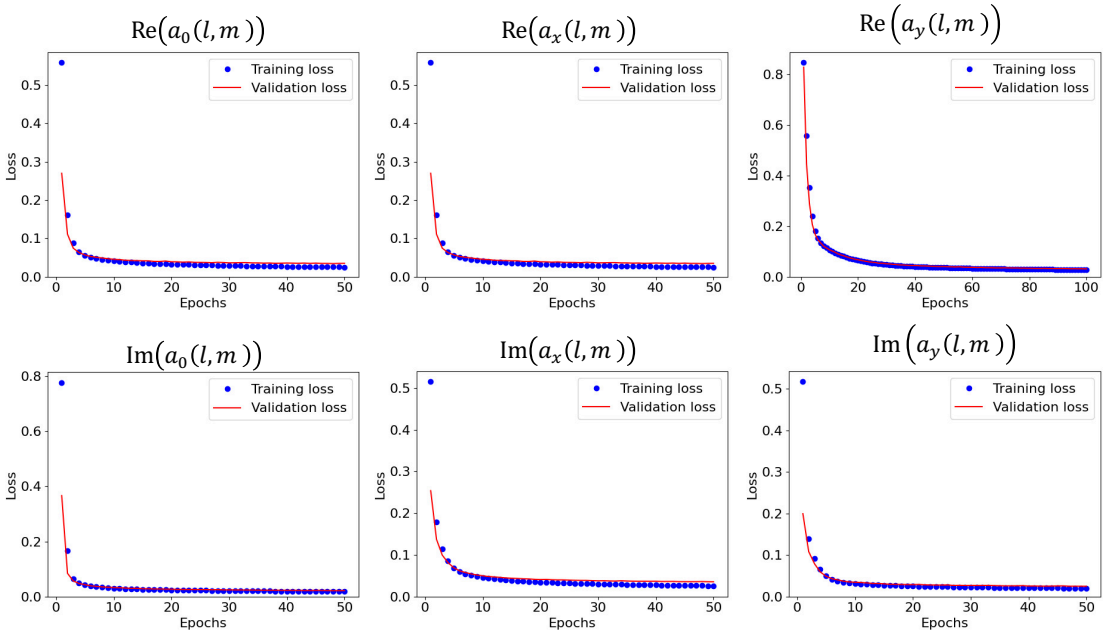

Fig. 4: Training and validation losses of CNNs.

C. Accuracy and speed of CNN

The image intensity $I(x,y)$ at wafer position (x,y) is defined as

$$I(x,y) = \iint S(s_x,s_y)\left|\widehat{\boldsymbol{A}}(x,y;s_x,s_y)\right|^2 \mathrm{d}s_x\mathrm{d}s_y,$$

$$\widehat{\boldsymbol{A}}(x,y;s_x,s_y) = \iint \widetilde{\boldsymbol{A}}(k_x,k_y;s_x,s_y)P(k_x,k_y)e^{-i(k_xx+k_yy)}\mathrm{d}k_x\mathrm{d}k_y$$

where $S(s_x,s_y)$ is the source intensity at the source position (s_x,s_y), $P(k_x,k_y)$ is the pupil function in terms of the wave vector (k_x,k_y) at the pupil, and $\widetilde{\boldsymbol{A}}(k_x,k_y;s_x,s_y)$ is the diffraction amplitude from source position (s_x,s_y) via the wave vector (k_x,k_y). $\widetilde{A}(k_x,k_y;s_x,s_y)$ is defined as

$$\widetilde{A}(k_x,k_y;s_x,s_y) = A^{\mathrm{FT}}(l,m) + A^{\mathrm{3D}}(l,m;l_s,m_s)$$

where $l = \left\lfloor (k_x - s_x)\frac{L}{2\pi}\right\rfloor$, $m = \left\lfloor (k_y - s_y)\frac{L}{2\pi}\right\rfloor$, $l_s = \left\lfloor s_x\frac{L}{2\pi}\right\rfloor$, $m_s = \left\lfloor s_y\frac{L}{2\pi}\right\rfloor$, and L is the mask pattern pitch for a periodic boundary condition [11].

Figure 5 shows root mean square (RMS) differences in the image intensities obtained by the EM simulation (EM) and that by two other methods (FT and CNN): the thin mask model using Fourier transform of the mask pattern without/with M3D effects predicted by CNN. The intensity difference between EM and CNN is significantly smaller than that between EM and FT. The RMS of the image intensity difference between the EM and FT is 2.5%, and the difference between EM and CNN is 0.9% [21].

The CNN prediction time for M3D parameters is 0.05 seconds, and the image intensity calculation takes 0.07 seconds, resulting in a total computation time of 0.12 seconds. This is approximately 3,000 times faster than the EM simulation [21].

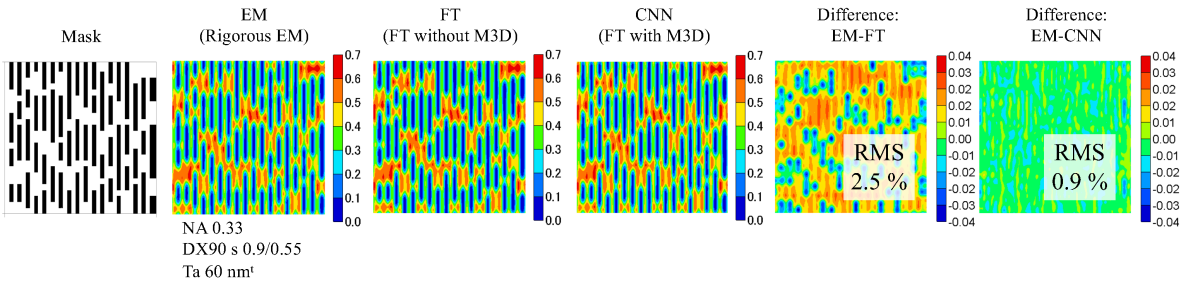

Fig. 5: Image intensity difference between EM and FT, and the difference between EM and CNN.

IV. Conclusion

CNN model is constructed to predict M3D parameters from an input mask pattern. CNN prediction successfully reproduces the result of EM simulation. The image intensity estimation by CNN prediction is 3,000 times faster than that by EM simulation. In our research, CNNs for Manhattan mask patterns were developed. There are limitations of the current CNNs on accuracy for other types such as curvilinear mask patterns. Our final goal is to build a universal CNN for arbitrary mask patterns.

Acknowledgments

This work was partially supported by JSPS KAKENHI Grant Number JP25K03090 and MEXT Initiative to Establish Next-generation Novel Integrated Circuits Centers (X-NICS) Grant Number JPJ011438.

References

[1] A. K.-K. Wong, *Resolution Enhancement Techniques in Optical Lithography*. SPIE press, 2001.

[2] J.-R. Gao, X. Xu, B. Yu, and D. Z. Pan, "MOSAIC: Mask optimizing solution with process window aware inverse correction," in *Proc. Design Automation Conference (DAC)*, pp. 1–6, 2014. doi:10.1145/2593069.2593163.

[3] L. Pang, "Inverse lithography technology: 30 years from concept to practical, full-chip reality," *Journal of Micro/Nanopatterning, Materials and Metrology (JM3)*, vol. 20, no. 3, pp. 030901–1–030901–49, 2021. doi:10.1117/1.JMM.20.3.030901.

[4] S. Sun, F. Yang, B. Yu, L. Shang, and X. Zeng, "Efficient ILT via multi-level lithography simulation," in *Proc. Design Automation Conference (DAC)*, pp. 1–6, 2023. doi:10.1109/DAC56929.2023.10247704.

[5] N. Nonaka, M. Kuramochi, Y. Kohira, R. Azuma, T. Matsui, A. Takahashi, and C. Kodama, "Fast mask optimization under process variation using guided local search on quadratic programming," *IEEE Transactions on Computer-Aided Design of Integrated Circuits and Systems (TCAD)*, vol. 44, 2025. doi:10.1109/TCAD.2025.3558148 (to appear).

[6] A. Awad, A. Takahashi, and C. Kodama, "A fast mask manufacturability and process variation aware OPC algorithm with exploiting a novel intensity estimation model," *IEICE Trans. Fundamentals*, vol. E99-A, no. 12, pp. 2363–2374, 2016. doi:10.1587/transfun.E99.A.2363.

[7] A. Awad, A. Takahashi, S. Tanaka, and C. Kodama, "Intensity difference map (IDM) accuracy analysis for OPC efficiency verification and further enhancement," *IPSJ Trans. on System LSI Design Methodology (TSLDM)*, vol. 10, pp. 28–38, 2017. doi:10.2197/ipsjtsldm.10.28.

[8] A. Awad, A. Takahashi, S. Tanaka, and C. Kodama, "A fast process variation aware mask optimization algorithm with a novel intensity modeling," *IEEE Transactions on Very Large Scale Integration Systems (TVLSI)*, vol. 25, no. 3, pp. 998–1011, 2025. doi:10.1109/TVLSI.2016.2616840.

[9] H. Tanabe, S. Sato, and A. Takahashi, "Fast 3D lithography simulation by convolutional neural network: POC study," in *Proc. SPIE 11518, Photomask Technology*, pp. 115180L–1–115180L–7, 2020. doi:10.1117/12.2575971.

[10] H. Tanabe, S. Sato, and A. Takahashi, "Fast 3D lithography simulation by convolutional neural network," in *Proc. SPIE 11614, Design-Process-Technology Co-optimization XV*, pp. 116140M–1–116140M–8, 2021. doi:10.1117/12.2583683.

[11] H. Tanabe, S. Sato, and A. Takahashi, "Fast euv lithography simulation using convolutional neural network," *Journal of Micro/Nanopatterning, Materials and Metrology (JM3)*, vol. 20, no. 4, pp. 041202–1–041202–14, 2021. doi:10.1117/1.JMM.20.4.041202.

[12] H. Tanabe and A. Takahashi, "Data augmentation in EUV lithography simulation based on convolutional neural network," in *Proc. SPIE 12052, DTCO and Computational Patterning*, pp. 120520T–1–120520T–7, 2022. doi:10.1117/12.2615267.

[13] H. Tanabe and A. Takahashi, "Data augmentation in extreme ultraviolet lithography simulation using convolutional neural network," *Journal of Micro/Nanopatterning, Materials and Metrology (JM3)*, vol. 21, no. 4, pp. 041602–1–041602–10, 2022. doi:10.1117/1.JMM.21.4.041602.

[14] H. Tanabe, A. Jinguji, and A. Takahashi, "Evaluation of CNN for fast EUV lithography simulation using iN3 logic mask patterns," in *Proc. SPIE 12495, DTCO and Computational Patterning II*, pp. 124951J–1–124951J–7, 2023. doi:10.1117/12.2659063.

[15] H. Tanabe, A. Jinguji, and A. Takahashi, "Evaluation of convolutional neural network for fast extreme ultraviolet lithography simulation using imec 3 nm node mask patterns," *Journal of Micro/Nanopatterning, Materials and Metrology (JM3)*, vol. 22, no. 2, pp. 024201–1–024201–11, 2023. doi:10.1117/1.JMM.22.2.024201.

[16] H. Tanabe, A. Jinguji, and A. Takahashi, "Accelerating EUV lithography simulation with weakly guiding approximation and STCC formula," in *Proc. SPIE 12750, International Conference on Extreme Ultraviolet Lithography*, pp. 127500D–1–127500D–8, 2023. doi:10.1117/12.2688029.

[17] H. Tanabe, A. Jinguji, and A. Takahashi, "Accelerating extreme ultraviolet lithography simulation with weakly guiding approximation and source position dependent transmission cross coefficient formula," *Journal of Micro/Nanopatterning, Materials and Metrology (JM3)*, vol. 23, no. 1, pp. 014201–1–014201–11, 2024. doi:10.1117/1.JMM.23.1.014201.

[18] H. Tanabe, A. Jinguji, and A. Takahashi, "Pre-training CNN for fast euv lithography simulation including M3D effects," in *Proc. SPIE 12954, DTCO and Computational Patterning III*, pp. 129540I–1–129540I–6, 2024. doi:10.1117/12.3009880.

[19] H. Tanabe, A. Jinguji, and A. Takahashi, "Weakly guiding approximation of a three-dimensional waveguide model for extreme ultraviolet lithography simulation," *Journal of the Optical Society of America A*, vol. 41, no. 8, pp. 1491–1499, 2024. doi:10.1364/JOSAA.516610.

[20] H. Tanabe and A. Takahashi, "Absorber dependence of M3D overlay errors in high-NA and hyper-NA EUV lithography," in *Proc. SPIE 13424, Optical and EUV Nanolithography XXXVIII*, pp. 134240Q–1–134240Q–6, 2025. doi:10.1117/12.3046583.

[21] H. Tanabe, M. Shimoda, and A. Takahashi, "Rigorous electromagnetic simulator for extreme ultraviolet lithography and convolutional neural network reproducing electromagnetic simulations," *Journal of Micro/Nanopatterning, Materials, and Metrology (JM3)*, vol. 24, no. 2, pp. 024201–1–024201–17, 2025. doi:10.1117/1.JMM.24.2.024201.